

# An Intrinsically Three-Dimensional Magnetic Reconnection Process in a Generalized Harris Sheet

Ping Zhu<sup>1,2</sup>, Arash Sangari<sup>2</sup>, Zechen Wang<sup>1</sup>, and Phillip Bonofiglo<sup>2</sup>

<sup>1</sup>*CAS Key Laboratory of Geospace Environment and Department of Modern Physics*

*University of Science and Technology of China*

*Hefei, Anhui 230026, PRC*

<sup>2</sup>*Department of Engineering Physics*

*University of Wisconsin-Madison*

*Madison, WI 53706, USA*

## Abstract

A magnetic reconnection process in the generalized Harris sheet has been revealed to be intrinsically three-dimensional both geometrically and dynamically despite the spatial invariance of the original current sheet in the equilibrium current direction. The spatial distribution and structure of the quasi-separatrix layers, as well as their temporal emergence and evolution, indicate that the associated magnetic reconnection can only occur in a three-dimensional geometry which is irreducible to a two-dimensional reconnection process. Such a three-dimensional reconnection process is induced by the nonlinear development of an ideal MHD ballooning instability in the generalized Harris sheet, which is itself an intrinsically three-dimensional dynamic process.

Magnetic reconnection is believed to play fundamental roles in the eruptive energy conversion processes that are ubiquitous in laboratory and natural plasmas. Traditionally magnetic reconnection has been often interpreted using two-dimensional (2D) models, such as those by Sweet-Parker and Petschek [1–4], even though in reality magnetic reconnection always takes place in a three-dimensional (3D) space (e.g. [5]). The two-dimensional reconnection models essentially assume or imply the invariance of the magnetic reconnection process in the third spatial dimension perpendicular to the reconnecting field lines. Such 2D-based scenarios for reconnection have been useful in interpreting and understanding of many phenomena in 3-dimensional spatial domains. However, it remains a fundamental question whether all magnetic reconnection in 3D space can be reduced to a 2D process.

Recent simulations have found a plasmoid formation process in the generalized Harris sheet that is often used as a proxy to the configuration of the near-Earth magnetotail prior to a substorm onset [6, 7], where the magnetic configuration can be defined in a Cartesian coordinate system as  $\mathbf{B}_0(x, z) = \mathbf{e}_y \times \nabla \Psi(x, z)$ ,  $\Psi(x, z) = -\lambda \ln \frac{\cosh \left[ F(x) \frac{z}{\lambda} \right]}{F(x)}$ ,  $\ln F(x) = - \int B_{0z}(x, 0) dx / \lambda$ , and  $\lambda$  is the characteristic width of the current sheet. The conventional Harris sheet is recovered when  $F(x) = 1$ . The configuration can be further specified with a particular  $B_z$  profile that features a minimum region along the  $x$  axis, which could correspond to an embedded thin current sheet (Fig. 1), such as those often found in global MHD simulations and inferred from satellite observations in the near-Earth magnetotail, for example.

Those previous simulations demonstrate that the embedded thin current is unstable to ballooning mode perturbations, and the nonlinear development of the ballooning instability is able to induce the onset of reconnection and the formation of plasmoids in the current sheet where there is no pre-existing X-point or X-line.

A peculiar feature of that reconnection process is that the reconnection geometry becomes no longer invariant along the equilibrium current direction, unlike in a conventional 2D reconnection process. For example, at a time after the formation of plasmoids, those field lines crossing the  $y = -90$  line in the  $z = 0$  plane sees totally different plasmoid structure from the field lines crossing the  $y = -95$  line in the  $z = 0$  plane (Fig. 2). This leads to the general question as to where and how a reconnection takes place in the 3D configuration, as well as how the global structure of the 3D reconnection process can be characterized and

captured in manners different from the more familiar 2D reconnection process. More fundamentally, it had remained unclear whether this 3D reconnection process can be reducible to or interpretable in terms of the conventional 2D reconnection processes.

To address these questions in this work, we resort to the geometric concept of quasi-separatrix layer (QSL) that were previously developed for the analysis of the reconnection structures involved in the solar corona processes (e.g. [8, 9]). A quasi-separatrix layer is a region with steep gradient in the field line connectivity. QSL's are constructed by mapping field lines across a specified volume. A QSL is the region in which the gradient of this mapping is large compared to the average mapping. That is, QSL's define a region with a large change in mapping and squashing (defined in next section).

A surface,  $S$ , must first be defined to surround some volume of one's magnetic field. Divide  $S$  into two subspaces,  $S_0$  and  $S_1$ , where  $S_0$  represents the surface on which field lines enter the volume, and  $S_1$  represents those that leave. The initial footpoint is defined as  $(u_0, v_0)$  in  $S_0$ . One then traces the field line from the initial footpoint through the enclosed volume until the field line leaves the volume through  $S_1$  at the point  $(u_1, v_1)$ . The Jacobian transformation matrix and the norm of the mapping from  $(u_0, v_0)$  to  $(u_1, v_1)$  are defined as

$$\mathcal{J} = \begin{pmatrix} \frac{\partial u_1}{\partial u_0} & \frac{\partial u_1}{\partial v_0} \\ \frac{\partial v_1}{\partial u_0} & \frac{\partial v_1}{\partial v_0} \end{pmatrix} \quad (1)$$

$$N = \sqrt{\left(\frac{\partial u_1}{\partial u_0}\right)^2 + \left(\frac{\partial u_1}{\partial v_0}\right)^2 + \left(\frac{\partial v_1}{\partial u_0}\right)^2 + \left(\frac{\partial v_1}{\partial v_0}\right)^2}. \quad (2)$$

where a QSL is defined by the field lines for which  $N \gg 1$ .

The squashing degree  $Q$  is a dimensionless parameter that describes QSL's, which is representative of the squashing, or deformation, of flux tubes [9]. Mathematically, the squashing degree  $Q$  is defined as  $Q = N^2/|\Delta|$  where  $\Delta$  is the determinant of the Jacobian matrix. Geometrically, the squashing degree represents the area produced by the eigenvectors of the transformation matrix  $\mathcal{J}$ , which are related to the major and minor axes of the elliptical cross-section of the flux tube [9, 10].  $Q$  is invariant along a field line and has a minimum value of 2. The variation of  $Q$  among different field lines reflects the deformation of the magnetic flux tubes. A high squashing degree corresponds to a contraction in the cross-sectional area of a flux tube. Quasi-separatrix layers are the 3D extension to separatrices. The 2D projections of quasi-separatrix layers turn into separatrices in the limit the layer

thickness goes to zero, or the corresponding squashing factor goes to infinity. The physical significance of QSL is that current sheets may form on these layers for reconnection.

Another closely related geometric concept is bald Patch (BP). A BP is a group of points on the inversion line that separates regions of positive and negative polarity at the plane of mapping, where a magnetic field line becomes tangent to the plane and the concavity of the field line directs upward from the mapping plane [8, 11]. Mathematically a BP is defined as the region of a magnetic field that satisfies the condition  $(\mathbf{B}_\perp \cdot \nabla_\perp B_n)|_{IL} > 0$ , where  $\perp$  corresponds to the horizontal components within the mapping plane, the direction  $n$  is taken normal to the mapping plane, and  $IL$  denotes the inversion line where this is evaluated. The concept of BP has long been applied to the analyses of the magnetic field structure on solar photosphere [8, 9]. As shown later, the boundary of a BP, as defined in  $(\mathbf{B}_\perp \cdot \nabla_\perp B_n)|_{IL} = 0$ , can be used to designate the location of separatrices and separatrix surfaces, or quasi-separatrix layers formed during the 3D magnetic reconnection process in magnetotail as well.

From the mathematical definitions of BP's, QSL's, and squashing degrees, it is relatively straightforward to see their connection. Bald patches represent locations on inversion lines over which field lines do not cross from positive to negative polarity. Instead, field lines come down tangent to the mapping plane and bend back in a concave upward fashion with respect to the norm of the plane. On the other hand, QSL's are defined where the norm  $N$  becomes very large. This occurs where the gradient in the mapping is very steep. Now defining one side of our surface,  $S_0$ , as the inversion plane (which is composed of all the inversion lines), one can see that  $N$  will be very large near the boundary of bald patches because a small displacement in the horizontal direction within the surface  $S_0$  will cause a very large split in directions of field lines near the normal direction. This is a direct result of the field lines being tangential to the points on the boundary of a BP. All other points along the inversion plane will follow normal field line trends, resulting in small gradients and norms  $N$  from the field-line mappings [12]. Thus, the boundary of a bald patch is the region of “instability” in the gradient of the mapping. In this manner, we can expect the formation of quasi-separatrix layers around BP's.

In this work, we compute both the bald patches and the squashing degrees to identify the quasi-separatrix layers of the magnetic field configuration associated with the plasmoid formation, in an attempt to understand the global geometry of the magnetic field and the

3D nature of the magnetic reconnection process in association with the plasmoid formation process induced by ballooning instability.

We first briefly describe the development of bald patches in the inversion plane of the current sheet (i.e.  $z = 0$  plane) during the course of the ballooning instability evolution, as shown in Fig. 3. The inversion plane would correspond to the equatorial plane in a model for the near-Earth plasma sheet. In the initial and early stage of ballooning instability evolution, bald patches are absent in the  $z = 0$  plane ( $t = 170$ ) (Fig. 3, upper left). By the time  $t = 180$  the first set of bald patches shown as the region enclosed by their boundaries depicted as the white circles start to form periodically along the  $y$  direction within the  $z = 0$  plane around the line of  $x = 9.5$  (Fig. 3, upper right).

As the ballooning instability continues to evolve, a second set of bald patches start to form in the equatorial plane near the radially extending fronts of ballooning fingers around  $x \lesssim 13.5$  ( $t = 190$ ) (Fig. 3, middle left). The circular shape of each of these BP's is smaller in radius. Their spatial distribution pattern is similar to the first set of BP circles, but their locations are shifted in  $y$  direction from the first set by one half distance between two adjacent BP circles. After reaching their maximum sizes, the first set of BP circles begin to shrink into ellipses squeezed in the  $x$  direction and eventually disappear ( $t = 220 - 260$ ) (Fig. 3, middle right, lower left, and lower right). In addition, the locations of the BP circles also evolve, particularly for the second set. As the ballooning finger tips extend in the positive  $x$  direction, the BP circles behind the each finger tip in the second set move along in the same direction.

Furthermore, as the first set of BP circles nearly shrink into disappearance, a third set of BP circles start to emerge at  $x = 11$  between the first two sets around  $t = 240$  (Fig. 3, lower left). This set of BP circles later become dominant in size after the first set disappear and the second set also shrink in size. Different from the first set, the third set of BP circles have the same locations in  $y$  as those in the second set.

The spatial distribution of the QSL's indicated by these BP circles reveals the global 3D geometry of the associated plasmoid formation and reconnection processes. In particular, the locations of the QSL's are exactly where the plasmoids are found to develop. Take the time slices of  $t = 180, 220, 260$  for example, which correspond to the time moments of the panels in the right column of Fig. 3. At each of the 3 moments, we trace the magnetic field lines from the line  $y = -90, z = 0$  and the line  $y = -95, z = 0$ , and show the field line

structure in the left and the right columns of Fig. 4, respectively.

For those field lines whose crossing points in equatorial plane are away from the QSL's, the field line structure and connectivity remain topologically same as the beginning. One of such a case is shown in Fig. 4 (upper left) where all the field lines cross the  $z = 0$  plane through the line  $y = -90, z = 0$  at  $t = 180$ . After the QSL's appear near the ballooning finger tip around  $x = 13.5, y = -90, -80, \dots$  in the  $z = 0$  plane at  $t = 220$ , a small plasmoid is spotted to form around  $x = 13.5$  on those same field lines across the  $y = -90, z = 0$  line (Fig. 4, middle left). At a later time ( $t = 260$ ), whereas that plasmoid has moved slightly toward the positive  $x$ -direction, a larger plasmoid appears on the same line of  $y = -90$  in the  $z = 0$  plane, but at a location around  $x = 10.5$  much behind that of the smaller plasmoid (Fig. 4, lower left). The BP plot at the same time shows the emergence of a set of larger circle-shaped QSL's around the line  $x = 10.5, z = 0$  along the  $y$  direction (Fig. 3, lower right). Similarly, for those field lines crossing the line  $y = -95, z = 0$ , which is half wavelength of the dominant linear ballooning instability in the  $y$ -direction away from the field lines in the previous case in the  $z = 0$  plane, the appearance of plasmoids in Fig. 4 (right column) conforms exactly with the emergence of QSL's as indicated by the BP contours in Fig. 3 (right column) in both time and location.

Our calculations find that the QSL's identified from the BP contours agree with those from the contours of squashing degrees. For example, the QSL's represented by the dark-lined circles in Fig. 5 which are centered around  $x = 9.5, y = -95$  and  $x = 13.4, y = -90$ . They have essentially the same shapes and locations as the QSL's represented by the white circles in Fig. 3 for the same time moment ( $t = 19$ ). The size and shape of the QSL's correspond to those of the plasmoids in the 2D  $x - z$  plane as projected to from the flux ropes in 3D.

The periodic distribution of QSL's in the  $y$ -direction indicates that the underlying reconnection process cannot take place in a two-dimensional domain where the  $y$ -direction is totally symmetric or invariant. Unlike a 2D reconnection process, X-line no longer exist in such a 3D reconnection; the X-line is broken into disconnected X-points in the  $y$ -direction. The intrinsic 3D nature of the reconnecting field line geometry originates from the intrinsic 3D dynamics of the reconnection process. As shown previously, the formation of plasmoids in the generalized Harris sheet considered here is induced by the nonlinear development of ballooning instability [6, 7]. Because the ballooning instability can only grow into nonlinear

stage with a finite wavenumber in  $y$ -direction (i.e.  $k_y \neq 0$ ), the dynamics of plasmoid formation and reconnection process induced by the nonlinear ballooning instability is inherently 3D in nature and cannot take place in any 2D configuration space. In another word, there is no equivalent 2D reconnection process that the 3D reconnection described in this paper can reduce to.

In summary, a magnetic reconnection process in the generalized Harris sheet has been revealed to be intrinsically three-dimensional both geometrically and dynamically despite the spatial invariance of the original current sheet in the equilibrium current direction. The intrinsic geometrical three-dimensionality of the reconnection process is a direct consequence of the intrinsic 3D nature of its MHD driver, i.e. ballooning instability. Due to the ubiquitous presence of 3D MHD instabilities and their associated reconnection processes in space and fusion plasmas, it may be more insightful to interpret the associated observations beyond the commonly adopted paradigm of 2D reconnection .

This research was supported by Natural Science Foundation of China grant No. 41474143, U.S. NSF grant No. AGS-0902360, and the 100 Talent Program of Chinese Academy of Sciences. The computational work used the NSF XSEDE resources provided by TACC under grant number TG-ATM070010, and the resources of NERSC, which is supported by DOE under Contract No. DE-AC02-05CH11231.

---

[1] P. A. Sweet, in *Electromagnetic Phenomena in Cosmical Physics, Proceedings from International Astronomical Union Symposium* (Cambridge University Press, London, 1958), vol. 6, p. 123, edited by Bo Lehnert.

[2] P. A. Sweet, *Nuovo Cimento Suppl.* **8**, Ser. X, 188 (1958).

[3] E. N. Parker, *Astrophys. J. Suppl. Ser.* **8**, 177 (1963).

[4] H. E. Petschek, in *AAS/NASA Symposium on the Physics of Solar Flares*, ed. W. N. Hess (NASA, Washington, DC, 1964), pp. 425–37.

[5] D. I. Pontin, *Adv. Space Res.* **47**, 1508 (2011).

[6] P. Zhu and J. Raeder, *Phys. Rev. Lett.* **110**, 235005 (2013).

[7] P. Zhu and J. Raeder, *J. Geophys. Res. Space Physics* **119**, 131 (2014).

[8] V. S. Titov and P. Démoulin, *Astron. Astrophys.* **351**, 707 (1999).

- [9] V. S. Titov and G. Hornig, *J. Geophys. Res.* **107**, 1164 (2002).
- [10] E. R. Priest and P. Demoulin, *J. Geophys. Res.* **100**, 23443 (1995).
- [11] V. S. Titov, E. R. Priest, and P. Demoulin, *Astron. Astrophys.* **276**, 564 (1993).
- [12] P. Demoulin, J. C. Henoux, E. R. Priest, et al., *Astron. and Astrophys.* **308**, 643 (1996).

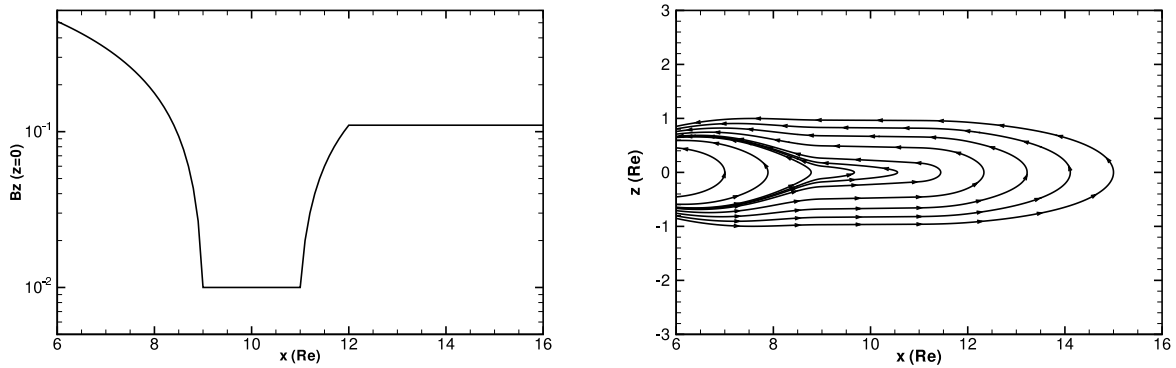


FIG. 1:  $B_z(x, z = 0)$  profile (left) and magnetic field lines (right) of a generalized Harris sheet.

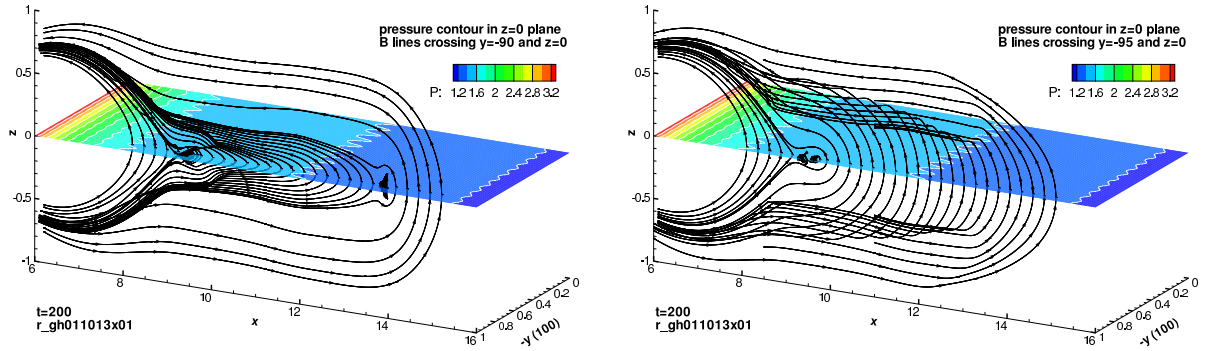


FIG. 2: Magnetic field lines crossing lines  $y = -90, z = 0$  (left) and  $y = -95, z = 0$  (right), and pressure contours in the  $z = 0$  plane at  $t = 200$ .

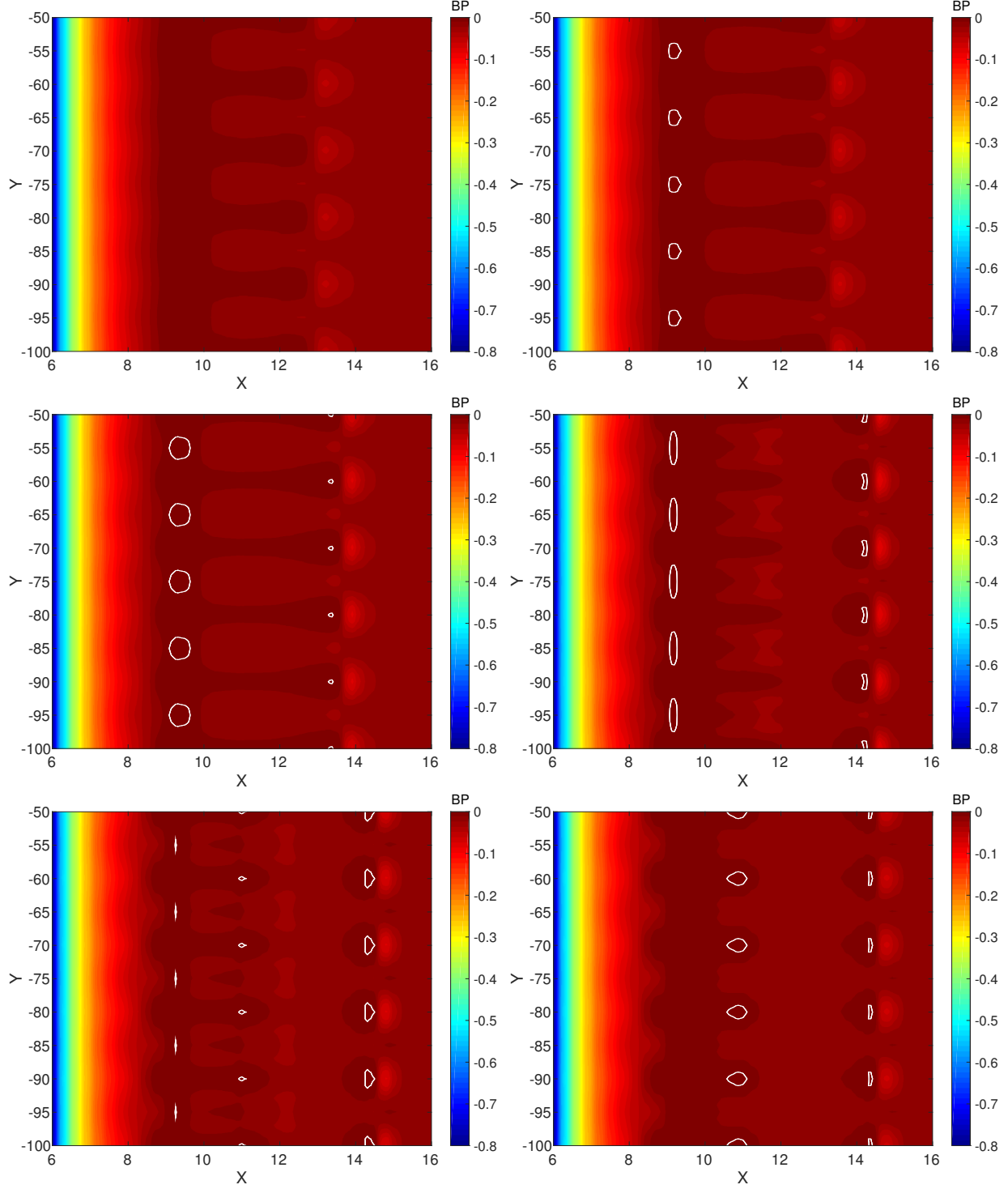


FIG. 3: Contours of  $(\mathbf{B}_\perp \cdot \nabla_\perp B_n)|_{IL}$  in  $z = 0$  plane at  $t = 170$  (upper left),  $t = 180$  (upper right),  $t = 190$  (middle left),  $t = 220$  (middle right),  $t = 240$  (lower left),  $t = 260$  (lower right). White circles denote the locations where  $(\mathbf{B}_\perp \cdot \nabla_\perp B_n)|_{IL} = 0$ . BP's are inside the white circles where  $(\mathbf{B}_\perp \cdot \nabla_\perp B_n)|_{IL} > 0$ .

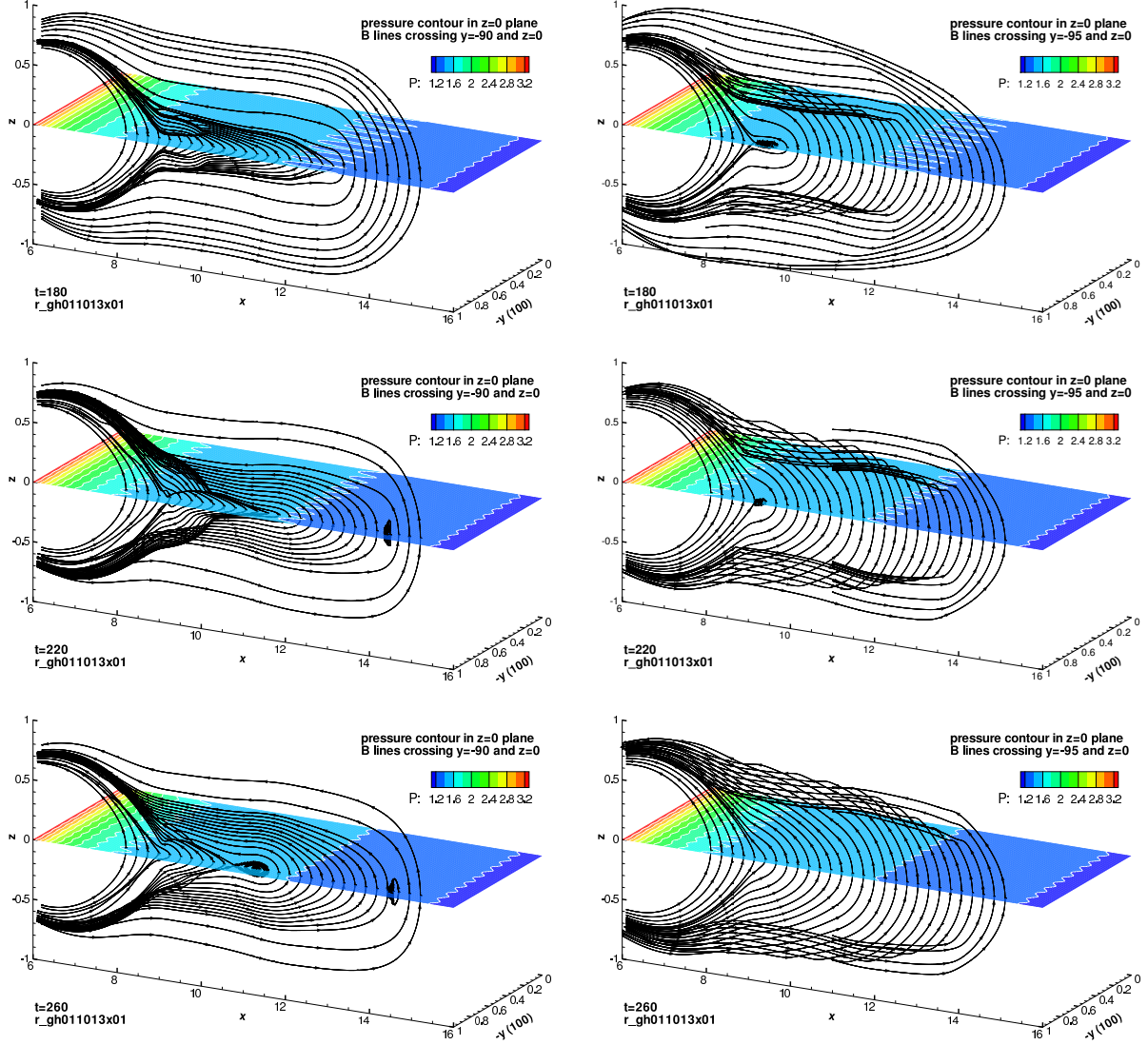


FIG. 4: Magnetic field lines crossing the line  $y = -90, z = 0$  (left) and the line  $y = -95, z = 0$  (right) at  $t = 180$  (upper),  $t = 220$  (middle), and  $t = 260$  (lower).

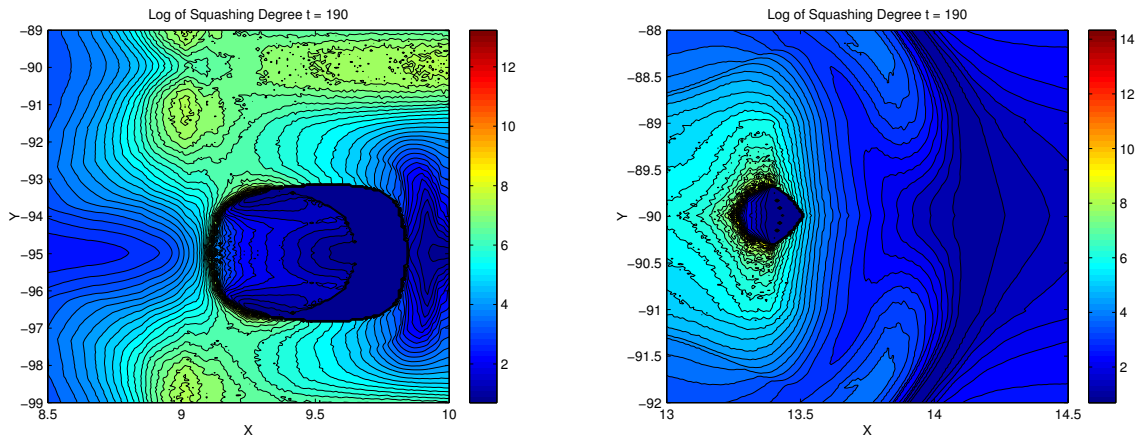


FIG. 5: Contours of the logarithm of squashing degree in the  $z = 0$  plane around  $x = 9.5, y = -95$  (upper) and  $x = 13.4, y = -90$  (lower) at  $t = 190$ .